Strong suppression of electron convection in Dirac and Weyl semimetals

P. O. Sukhachov,[1,*] E. V. Gorbar,[2,3] and I. A. Shovkovy[4,5]

[1] *Department of Physics, Yale University, New Haven, Connecticut 06520, USA*
[2] *Department of Physics, Taras Shevchenko National Kyiv University, Kyiv, 03022, Ukraine*
[3] *Bogolyubov Institute for Theoretical Physics, Kyiv, 03143, Ukraine*
[4] *College of Integrative Sciences and Arts, Arizona State University, Mesa, Arizona 85212, USA*
[5] *Department of Physics, Arizona State University, Tempe, Arizona 85287, USA*

(Dated: September 28, 2021)

It is shown that the convective instability in electron fluids in three- and two-dimensional (3D and 2D) Dirac and Weyl semimetals is strongly inhibited. The major obstacles for electron convection are the effects of the Coulomb forces and the momentum relaxation related to the interaction with impurities and phonons. The effect of the Coulomb forces is less pronounced in 2D materials, such as graphene. However, momentum relaxation still noticeably inhibits convection making it very difficult to achieve in practice.

Introduction.— Electron hydrodynamics is an unusual transport regime that can be realized in clean crystals. As first conjectured by Gurzhi in the 1960s [1, 2], electrons could form a hydrodynamic fluid when the electron-electron scattering rate is larger than the scattering rates of electrons on impurities and phonons. In such a regime, the electron transport should reveal some conventional hydrodynamic effects, including the Poiseuille-like profile of the current in a wire, the formation of vortices, etc.

Historically, a hydrodynamic electron flow was first observed in a two-dimensional (2D) electron gas of high-mobility (Al, Ga)As heterostructures [3, 4]. Later, a similar regime was confirmed in the ultrapure 2D metal palladium cobaltate ($PdCoO_2$) [5] and graphene [6–12]. (For reviews on electron hydrodynamics, see Refs. [13, 14].) Electron hydrodynamics in graphene could be experimentally revealed via a negative nonlocal resistance and the formation of current vortices [15–19], higher than ballistic conduction in constrictions [8, 20], and certain collective modes [21–24]. The profile of electric currents in the hydrodynamic regime can be reconstructed from the stray magnetic fields [11] or the Hall field across the graphene ribbon [12]. Recently, evidence of three-dimensional (3D) relativisticlike hydrodynamic electron transport was reported in the Weyl semimetal tungsten diphosphide WP_2 [25]. This shows that Dirac and Weyl semimetals provide another promising platform for investigating the hydrodynamic regime of the electron transport in solids.

Dirac and Weyl semimetals are novel materials whose electron quasiparticle spectrum is described by the corresponding equations in the vicinity of the band-crossing points known as Dirac points and Weyl nodes [26–28], respectively. Representative material realizations of Dirac semimetals include A_3Bi (A = Na, K, Rb) [29, 30] and Cd_3As_2 [31–33] in 3D, as well as graphene in 2D. Weyl semimetals are realized, e.g., in transition metal monopnictides (TaAs, TaP, NbAs, and NbP) [34–40], $EuCd_2As_2$ [41, 42], $Co_3Sn_2S_2$ [43–45], etc.

Guided by experience with conventional fluids, one may expect similar hydrodynamic effects to show up in the electron fluid. For example, the possibility of a preturbulent regime in graphene was proposed in Refs. [46, 47]. (Kagome metals may provide a compelling platform for realizations of turbulence in electron fluids [48].) The formation of the Rayleigh-Bénard convective cells in graphene was suggested and numerically studied in Ref. [49]. Generally, the Rayleigh-Bénard instability occurs in fluids subject to a buoyancy force (e.g., caused by gravity) and temperature gradient that results in a local thermal expansion of fluid [50, 51]. If the buoyancy force is strong enough, it becomes favorable to develop regular convective cells where the heat transfer is greatly assisted by the fluid motion. The observation of such cells would be a definitive signature of electron hydrodynamics. The possibility of electron convection is not only of academic interest but also can have important practical applications. Indeed, the convective regime may be invaluable for an effective heat transfer because the Nusselt number, which quantifies the ratio of convective to conductive heat transfer, is up to 10 (1000) times larger for a laminar (turbulent) flow. Since there are significant differences between conventional fluids and electron plasma in semimetals, it is necessary to investigate the onset conditions for electron convection in detail.

In this Letter, we show that the Rayleigh-Bénard instability in electron fluids in Dirac and Weyl semimetals is *strongly inhibited*. We identify two major obstacles for the electron fluid convection: (i) Coulomb forces and (ii) momentum-relaxation effects. Unlike many conventional fluids, the electron plasma is electrically charged. In a semimetal, the overall electric neutrality is preserved by the compensating charge of immovable lattice ions. Any deviation from local neutrality induces a strong electric field and, consequently, is energetically unfavorable. In other words, the effects of the Coulomb forces strongly suppress local expansion and compression of the electron fluid. For the same reason, a temperature gradient cannot easily induce sufficiently large local density devia-

tions needed for triggering convection.

We support this qualitative argument by a quantitative estimate of the Rayleigh number. Due to the aforementioned obstacles, the latter is so large in 3D Dirac and Weyl semimetals that achieving convection becomes practically impossible under any realistic conditions. As one might expect, the effects of the Coulomb forces are less pronounced in 2D materials. However, due to ubiquitous disorder effects and interaction with phonons, the momentum relaxation also noticeably inhibits a convective flow in both 2D and 3D systems.

Model.— The starting point in our discussion of the electron fluid is the Navier-Stokes equation [13, 14],

$$\frac{1}{v_F^2}\left[\partial_t(\mathbf{u}w)+\mathbf{u}w(\boldsymbol{\nabla}\cdot\mathbf{u})+(\mathbf{u}\cdot\boldsymbol{\nabla})(\mathbf{u}w)\right]-\eta\Delta\mathbf{u} - \left[\zeta+\frac{\eta(d-2)}{d}\right]\boldsymbol{\nabla}\left(\boldsymbol{\nabla}\cdot\mathbf{u}\right)=-\boldsymbol{\nabla}P-\frac{w\mathbf{u}}{v_F^2\tau}-en\mathbf{E}. \tag{1}$$

Here, $w=\epsilon+P$ is the enthalpy, ϵ is the energy density, P is the pressure, $\mathbf{u}$ is the electron fluid velocity, n is the electron number density, $-e$ is the electron charge, and v_F is the Fermi velocity. Further, η and ζ are the shear and bulk viscosities, respectively. In relativisticlike systems, $\zeta\approx 0$ [52] and $\eta=\eta_{\rm kin}w/v_F^2$, where $\eta_{\rm kin}\sim v_F^2\tau_{\rm ee}$ is the kinematic shear viscosity and $\tau_{\rm ee}$ is the electron-electron interaction time (see, e.g., Refs. [53, 54]). For a relativisticlike fluid, $P=\epsilon/d$ and $w=(d+1)\epsilon/d$, where d is the spatial dimension. The momentum relaxation, which is inevitable in real solids, is quantified by the relaxation time τ that contains contributions from scattering on impurities and phonons. For simplicity, we assume that the electron fluid is isotropic, which is sufficient for the purposes of this study. Finally, we account for an electric field $\mathbf{E}$, which includes both external and induced contributions.

The electric and energy current densities are

$$\mathbf{J}=-en\mathbf{u}+\sigma\left[\mathbf{E}+\frac{T}{e}\boldsymbol{\nabla}\left(\frac{\mu}{T}\right)\right], \tag{2}$$

$$\mathbf{J}^{\epsilon}=w\mathbf{u}-\eta\left[\left(\boldsymbol{\nabla}\cdot\mathbf{u}\right)\mathbf{u}+u_j\boldsymbol{\nabla}u_j-\frac{2}{d}\mathbf{u}\left(\boldsymbol{\nabla}\cdot\mathbf{u}\right)\right]. \tag{3}$$

Here, μ is the chemical potential, T is temperature, and σ is the intrinsic conductivity [13]. The electric and energy currents satisfy the standard continuity relations

$$-e\partial_t n+\left(\boldsymbol{\nabla}\cdot\mathbf{J}\right)=0 \tag{4}$$

and

$$\partial_t\epsilon+\left(\boldsymbol{\nabla}\cdot\mathbf{J}^{\epsilon}\right)=\left(\mathbf{E}\cdot\mathbf{J}\right), \tag{5}$$

respectively.

Since the electron fluid is electrically charged, the hydrodynamic equations should be supplemented by Maxwell's equations. By assuming a slow flow, we neglect the effects of dynamic magnetic fields on fluid motion. In such a quasistatic approximation, only the Gauss law

$$\boldsymbol{\nabla}\cdot\mathbf{E}=-4\pi e\delta n \tag{6}$$

is relevant. Here, $-e\delta n$ is the deviation of the electron charge density from the background equilibrium value. As we will show below, electric fields induced by δn play a profound role in suppressing electron convection in 3D. The Coulomb forces also hinder convection in 2D systems, but their effect is less dramatic.

It is worth noting that the Coulomb interactions are responsible for both viscosity of the electron fluid and screening effects. Indeed, it is the microscopic interparticle Coulomb force that governs the electron-electron scattering and the formation of electron fluid. On the other hand, the Gauss law in Eq. (6) determines a background electric field, which comes as an average uncompensated field over macroscopic distances. This field is induced when the electron fluid is compressed or expanded locally with respect to the ion lattice.

To investigate the possibility of electron convection, we follow the same conceptual approach as in conventional fluids (see, e.g., Refs. [55, 56]), but amend the hydrodynamic equations with the Gauss law. As the first step, we find the steady-state solutions for the temperature profile and the electric field in the absence of hydrodynamic flow. Then, by using these solutions as a background, we derive the threshold criterion for convection.

Steady-state solution without flow.— Let us start by determining the steady-state solution for the electric field and temperature inside a slab of finite thickness L along the x direction. For simplicity, we assume that the slab is infinite along other directions.

Temperature $T(x)$ and the electric potential $\varphi(x)$ take different values on the opposite surfaces of the slab, i.e.,

$$T(x=0)=T_{\rm L},\qquad T(x=L)=T_{\rm R}, \tag{7}$$

$$\varphi(x=0)=\varphi_{\rm L},\qquad \varphi(x=L)=\varphi_{\rm R}. \tag{8}$$

We employ a perturbation scheme where deviations of all quantities (denoted by a tilde) are small compared to their global equilibrium values (denoted by subscript 0), e.g., $\tilde{T}/T_0\ll 1$, etc. By setting $\mathbf{u}=\mathbf{0}$ in Eqs. (1) through (6), one finds that the temperature function $\tilde{T}(x)$ is determined by the Laplace equation, $\Delta\tilde{T}=0$. Its solution that satisfies the boundary conditions (7) reads

$$\tilde{T}=T_{\rm L}-T_0+\frac{T_{\rm R}-T_{\rm L}}{L}x. \tag{9}$$

By taking into account this solution, Eqs. (4) and (6) can be rewritten as follows:

$$\Delta\tilde{\mu}=4\pi e^2\tilde{n}=q_{\rm TF}^2\tilde{\mu}+4\pi e^2(\partial_T n)\tilde{T}, \tag{10}$$

$$\Delta\tilde{\varphi}=-4\pi e\tilde{n}, \tag{11}$$

where $q_{\rm TF}=\sqrt{4\pi e^2(\partial_\mu n)}$ is the Thomas-Fermi wave vector. Its explicit expression is given in the Supplemental Material [57].

By using the equation of motion (1) at $\mathbf{u}=\mathbf{0}$ and requiring the overall charge neutrality of the sample, we obtain the steady-state expressions for $\tilde{\mu}$ and $\tilde{\varphi}$ (see Supplemental Material [57]). They reveal that the electric field is nonvanishing but screened strongly inside the sample. Also, the electric charge deviations are small ($\tilde{n}\approx 0$) in the bulk of the slab. However, both electric field and charge density are noticeably nonuniform near the surfaces. Since convection is determined largely by bulk properties, it is justified to ignore the inhomogeneity of the electric field and other variables near the surfaces. Such an approximation simplifies analytical calculations but should not affect the qualitative results for sufficiently thick samples.

Convection threshold.— To determine the threshold of convection, we consider a hydrodynamic flow in the background of the screened electric field and the temperature gradient obtained in the previous section. As in conventional fluids [55, 56], the analysis is simplified by using an analog of the Oberbeck-Boussinesq approximation. The resulting system, which is linear in the flow velocity $\mathbf{u}$ and the flow-driven deviations P_u, $\mathbf{E}_u$, n_u, μ_u, and T_u (appearing on top of the steady-state solution), reads

$$\boldsymbol{\nabla}P_u-\eta\Delta\mathbf{u}-\left[\zeta+\frac{\eta(d-2)}{d}\right]\boldsymbol{\nabla}\left(\boldsymbol{\nabla}\cdot\mathbf{u}\right)=-\frac{w_0\mathbf{u}}{v_F^2\tau}-en_0\mathbf{E}_u-en_u\tilde{\mathbf{E}}, \tag{12}$$

$$(\mathbf{u}\cdot\boldsymbol{\nabla})\tilde{w}+w_0(\boldsymbol{\nabla}\cdot\mathbf{u})=0, \tag{13}$$

$$-en_0(\boldsymbol{\nabla}\cdot\mathbf{u})+\sigma(\boldsymbol{\nabla}\cdot\mathbf{E}_u)+\frac{\sigma}{e}\left(\Delta\mu_u-\frac{\mu_0}{T_0}\Delta T_u\right)=0, \tag{14}$$

$$\boldsymbol{\nabla}\cdot\mathbf{E}_u=-4\pi en_u. \tag{15}$$

Here, we assumed that the cross-terms containing fluid flow velocity and the temperature gradient are small compared to other terms. In addition, we neglected the terms that are of the second order in steady-state deviations (e.g., $\tilde{n}\tilde{\mathbf{E}}\ll n_0\tilde{\mathbf{E}}$).

The last term on the right-hand side in Eq. (12) and the first term in Eq. (13) are crucial for driving convection and their analogs are included in the Oberbeck-Boussinesq approximation for conventional fluids. Indeed, the term $-en_u\tilde{\mathbf{E}}$ is similar to the buoyancy force for regular fluids. Recall that buoyancy is the consequence of an external (e.g., gravitational) force exerted on a fluid with a density gradient, typically induced by a temperature difference between the top and bottom surfaces. In the case of electrons, gravitation has negligible effects and the role of buoyancy force is played by the electric force related to the in-medium electric field $\tilde{\mathbf{E}}$. Therefore, another key requirement for achieving convection is the nonzero compressibility of the fluid. It is taken into account by the first term in Eq. (13).

It is very important for the problem under consideration that, unlike ordinary fluids, expansion and compression of the electron fluid give rise to strong electric fields. Indeed, in view of the Gauss law (15), any change of the electric charge density leads to an electric field. As we will explicitly show below, this is one of the key factors inhibiting convection in electron fluids as the energy price for the appearance of electric fields is very high.

To estimate the threshold for convection, we use the bulk steady-state solutions, $\tilde{n}\approx 0$ and $\tilde{\mathbf{E}}=\tilde{E}\hat{\mathbf{x}}$, which include both external and induced fields. Then, $(\mathbf{u}\cdot\boldsymbol{\nabla})\tilde{w}=u_x(\partial_x\tilde{w})\propto u_x\left(T_R-T_L\right)$. The explicit expression for $(\partial_x\tilde{w})$ as well as the general solutions to Eqs. (12) through (15) are given in the Supplemental Material [57].

We use a plane-wave ansatz for the hydrodynamic variables u_x, T_u, and μ_u, e.g.,

$$T_u=C_Te^{i\mathbf{k}_\perp\cdot\mathbf{r}_\perp}e^{ik_xx}, \tag{16}$$

where $\mathbf{k}_\perp$ is the wave vector perpendicular to the surface normal. The characteristic equation for the system of Eqs. (12) through (15) reads [57]

$$k^2\left(k^2+\frac{1}{\lambda_G^2}\right)\left(k^2+q_{\mathrm{TF}}^2\right)-\frac{k_\perp^2}{L^4}\mathrm{Ra}=0, \tag{17}$$

where $k^2=k_\perp^2+k_x^2$. In Eq. (17), we used the following shorthand notations:

$$\lambda_G=\sqrt{\frac{v_F^2\tau\eta}{w_0}}=\sqrt{\tau\eta_{\mathrm{kin}}}, \tag{18}$$

$$\mathrm{Ra}=L^4\frac{e^3n_0\tilde{E}(\partial_x\tilde{w})T_0}{\sigma w_0^2\eta}\left[n_0(\partial_Tn)-s_0(\partial_\mu n)\right]. \tag{19}$$

Here, λ_G is the Gurzhi length that quantifies the momentum relaxation and Ra is the Rayleigh number. In the limit $\lambda_G\to\infty$ and $q_{\mathrm{TF}}\to 0$, the characteristic equation (17) coincides with the textbook result for conventional fluids (cf. Ref. [55]). Convective instability characterized by periodic spatial pattern of the fluid velocity is realized for real k_x and $k_\perp$. This requires $\mathrm{Ra}\gtrsim\mathrm{Ra}_{\mathrm{min}}$, where $\mathrm{Ra}_{\mathrm{min}}$ is determined from the characteristic equation (17) with wave vectors constrained by boundary conditions.

To derive the convection threshold $\mathrm{Ra}_{\mathrm{min}}$, let us determine the allowed values of k_x in Eq. (17). They follow from the boundary conditions for T_u and $\mathbf{u}$, i.e.,

$$T_u(x=0,L)=0,\quad u_x(x=0,L)=0. \tag{20}$$

For the perpendicular components of velocity $\mathbf{u}_\perp$, we employ the free-surface boundary conditions, which provide the most conservative estimate of the convection threshold. Indeed, the no-slip boundary conditions can be considered as a source of additional dissipation that further inhibits convection; see, e.g., Ref. [56] for neutral fluids. We found that the free-surface boundary conditions are satisfied for $|k_x|=\pi n/L$ with $n=1,2,3,\ldots$ (see Supplemental Material [57] for details). It is worth noting, however, that the exact form of the boundary conditions

is not important for our qualitative arguments because they only determine the allowed values of k_x.

The characteristic equation (17) gives the following relation between the Rayleigh number and wave vector:

$$\mathrm{Ra} = L^4 \frac{\left(k_\perp^2 + k_x^2\right)\left(k_\perp^2 + k_x^2 + \lambda_G^{-2}\right)\left(k_\perp^2 + k_x^2 + q_{\mathrm{TF}}^2\right)}{k_\perp^2}. \tag{21}$$

This shows that the Coulomb forces and the momentum relaxation effects, quantified by q_{TF} and λ_G, respectively, increase the minimal value of the Rayleigh number $\mathrm{Ra}_{\mathrm{min}}$ needed to achieve convection. In order to determine $\mathrm{Ra}_{\mathrm{min}}$, one should minimize Eq. (21) with respect to the wave vectors allowed by the boundary conditions, i.e., at $k_x = \pi/L$. The general expression for the minimal Rayleigh number at finite λ_G and nonzero q_{TF} is cumbersome (see also Supplemental Material [57]). Since the Rayleigh number Ra increases with k_x, we can estimate the corresponding lower bound Ra_0 (which is smaller than the actual $\mathrm{Ra}_{\mathrm{min}}$) by setting $k_x = 0$ and neglecting $k_\perp$ compared to q_{TF} and λ_G^{-1} in Eq. (21), i.e.,

$$\mathrm{Ra}_0 = L^4 q_{\mathrm{TF}}^2/\lambda_G^2 < \mathrm{Ra}_{\mathrm{min}}. \tag{22}$$

It is instructive to mention that $q_{\mathrm{TF}} \gg \pi/L$ and $\lambda_G \ll L/\pi$ hold for realistic samples of 3D Dirac and Weyl semimetals and, therefore, the above estimate is indeed reasonable. To verify this, let us consider typical parameters for semimetals, e.g., $\mu_0 = 20$ meV, $T_0 = 25$ K, and use the Fermi velocity $v_F \approx 1.4 \times 10^7$ cm/s [58]. In this case, one obtains $q_{\mathrm{TF}} \approx 9.9 \times 10^6$ cm^{-1} by assuming quasiparticles with a 3D relativisticlike energy spectrum. For such a large Thomas-Fermi wave vector, one finds that $q_{\mathrm{TF}} \gg \pi/L$ in a wide range of experimentally achievable samples [59]. As for the momentum relaxation length, we estimate $\lambda_G \approx 0.4$ μm at $\tau = 0.1$ ns and $\tau_{\mathrm{ee}} = 0.3$ ps, which is quite small compared to a typical thickness of Dirac semimetal slabs.

By using Eq. (22) and the same characteristic parameters as before, we estimate the lower bound for $\mathrm{Ra}_{\mathrm{min}}$ as

$$\mathrm{Ra}_0 = L^4 q_{\mathrm{TF}}^2/\lambda_G^2 \approx 6.5 \times 10^{22} \left(\frac{L}{1\ \mathrm{cm}}\right)^4. \tag{23}$$

It is instructive to compare this estimate with the benchmark result for conventional fluids. By taking $\lambda_G \to \infty$ and $q_{\mathrm{TF}} = 0$, we find that the critical value of the Rayleigh number is reached for $k_x = \pi/L$ and $k_{\perp,\mathrm{min}} = \pi/(\sqrt{2}L)$ giving $\mathrm{Ra}_{\mathrm{min}} = 27\pi^4/4 \approx 657.5$.

The enormous value of the lower bound for the minimal Rayleigh number (23) implies that convection in the electron fluid is strongly suppressed. Indeed, Eq. (19) gives the following estimate for the Rayleigh number in Dirac semimetals:

$$\mathrm{Ra} \approx 4 \times 10^9 \frac{\delta T}{T_0} \frac{\tilde{E}}{1\ \mathrm{V/m}} \left(\frac{L}{1\ \mathrm{cm}}\right)^3, \tag{24}$$

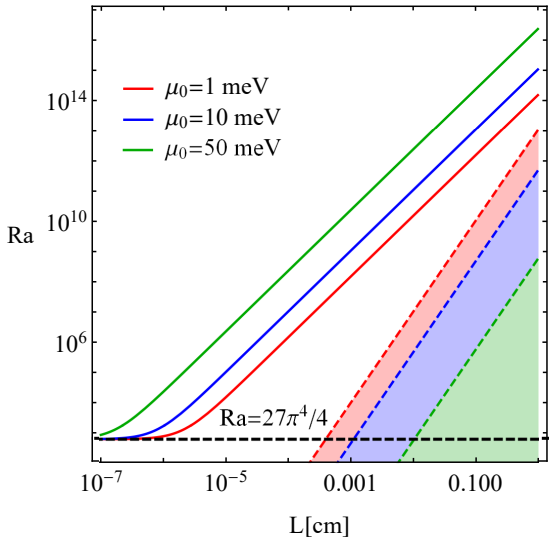

FIG. 1. Solid lines show the minimal Rayleigh number needed for convection. The realistic Rayleigh numbers achievable in Dirac semimetals are shown by the shaded regions. Dashed lines show the Rayleigh number (24) calculated for $\delta T = T_0$ and $\tilde{E} = 10$ V/m. The Gurzhi length is $\lambda_G \approx 0.4$ μm and the values of the Thomas-Fermi wave vector are $q_{\mathrm{TF}} \approx 2 \times 10^6$ cm^{-1} at $\mu_0 = 1$ meV, $q_{\mathrm{TF}} \approx 5.2 \times 10^6$ cm^{-1} at $\mu_0 = 10$ meV, and $q_{\mathrm{TF}} \approx 2.4 \times 10^7$ cm^{-1} at $\mu_0 = 50$ meV.

where $\tilde{E}$ is the in-medium field that includes both external and induced components, and $\delta T/T_0$ is the normalized temperature difference between the slab surfaces. As is easy to see, the estimate in Eq. (24) is many orders of magnitude smaller than Ra_0 for any reasonable electric field and temperature gradient available in experiments. Thus, in agreement with the heuristic arguments, convection is ruled out for 3D Dirac semimetals.

The minimal Rayleigh number $\mathrm{Ra}_{\mathrm{min}}$ as a function of the slab width L is presented by solid lines in Fig. 1 for the three fixed values of the chemical potential: $\mu_0 = 1$ meV (red), $\mu_0 = 10$ meV (blue), and $\mu_0 = 50$ meV (green) [60]. As we see, the minimal Rayleigh number needed for convection is enormous for macroscopic samples. It approaches the value in conventional fluids, i.e., $\mathrm{Ra}_{\mathrm{min}} = 27\pi^4/4$, only for extremely thin slabs. In the same figure, the shaded regions show the ranges of realistic estimates for the Rayleigh number obtained from Eq. (24) by assuming rather conservative values $\delta T \le T_0$ and $\tilde{E} \le 10$ V/m. It is clear that the realistic values of the Rayleigh number are many orders of magnitude smaller than $\mathrm{Ra}_{\mathrm{min}}$ required for convection.

Graphene.— In view of the great interest in electron hydrodynamics in graphene, let us re-examine whether the convective instability is possible in the 2D case. While the electron convection in graphene was already studied in Ref. [49], the effects of the Coulomb forces and the momentum dissipation were not taken into account. The screening effects in gated graphene can be

treated in the "gradual channel" approximation [61, 62] (see also Ref. [21]). In this approximation, the induced electric field is given by

$$\mathbf{E}_u = \frac{e}{C}\boldsymbol{\nabla} n_u, \tag{25}$$

where $C = \varepsilon/(4\pi L_g)$ is the capacitance per unit area, ε is the dielectric constant, and L_g is the distance to the gate. The minimum Rayleigh number is determined similarly to the 3D case considered above, but the Gauss law (15) is replaced by Eq. (25) (for details, see Supplemental Material [57]). We obtain

$$\mathrm{Ra} = L^4 \frac{\left(k_\perp^2 + k_x^2\right)^2 \left(k_\perp^2 + k_x^2 + \lambda_G^{-2}\right)\left(1+Q^2\right)}{k_\perp^2}, \tag{26}$$

where $Q = \sqrt{e^2(\partial_\mu n)/C}$. For $T_u \propto \sin(k_x x)$, the boundary conditions are satisfied for $|k_x| = \pi n/L$ and $n = 1, 2, 3, \ldots$. As in the 3D case, the Coulomb forces and momentum relaxation increase the minimal Rayleigh number needed to achieve convection.

Quantitatively, the effects of the Coulomb forces are much weaker in 2D. This is also supported by numerical estimates. Indeed, by using typical parameters for graphene, i.e., $v_F = 1.1 \times 10^8$ cm/s, $\mu_0 = 100$ meV, $T_0 = 100$ K, $L_g = 100$ nm, and $\varepsilon = 1$, we estimate $Q \approx 6.6$ (see Supplemental Material [57] for details). Therefore, the Coulomb forces increase $\mathrm{Ra}_{\mathrm{min}}$ only by about an order of magnitude. The momentum relaxation effects, on the other hand, are very important. We estimate $\lambda_G \approx 2.6$ μm at $\tau = 0.1$ ns and $\tau_{\mathrm{ee}} = (\hbar^2 v_F^2/e^4)(\hbar\mu_0/T_0^2) \approx 0.2$ ps. The corresponding minimal value of the Rayleigh number is

$$\mathrm{Ra}_{\mathrm{min}} \approx 2.7 \times 10^6 \tag{27}$$

at $L = 100$ μm. This is almost four orders of magnitude larger than the benchmark value $27\pi^4/4$. The Rayleigh number for graphene is estimated as

$$\mathrm{Ra} \approx 4.4 \times 10^7 \frac{\delta T}{T_0} \frac{\tilde{E}}{1\ \mathrm{V/m}} \left(\frac{L}{1\ \mathrm{cm}}\right)^3, \tag{28}$$

Our estimate suggests that in order to exceed the minimal Rayleigh number (27), centimeter-sized graphene samples are needed when the total electric fields are of the order of 1 V/m.

Thus, the momentum relaxation significantly inhibits convection in 2D systems too. The effect of the Coulomb forces, however, is less pronounced compared to the case of 3D Dirac semimetals. This situation resembles the role of the Coulomb forces in the spectrum of plasmons. Indeed, the plasmon dispersion relation is gapped in 3D due to the efficient screening of electric charge oscillations. On the other hand, in 2D systems the spectrum of plasmons remains gapless in the gradual channel approximation, where the Coulomb forces only enhance the plasma velocity.

Summary.— In this Letter, we showed that the convective instability is strongly inhibited in the electron fluid in 2D and 3D Dirac and Weyl semimetals. We identified the following two major inhibitors: (i) the Coulomb forces and (ii) the momentum relaxation effects due to scattering on impurities and phonons. Both are unavoidable and play a critical role in the charged electron fluid in semimetals. For realistic parameters in 3D Dirac and Weyl semimetals, the effect of the Coulomb forces dominates over the momentum relaxation and leads to an extremely large convection threshold. In 2D systems such as graphene, the key role is played by the momentum relaxation that increases the minimum Rayleigh number needed for convection. The corresponding threshold values are a few orders of magnitude larger than in conventional fluids. Our findings imply that the electron fluid convection is unlikely to be realized in Dirac and Weyl semimetals.

While we focused on the fluid of electron quasiparticles with an isotropic relativisticlike dispersion relation, similar arguments should apply to systems with anisotropic and even nonrelativisticlike dispersion relations, although the quantitative details will be different. For example, the critical value of the Rayleigh number may be different along different crystal directions for materials with anisotropic spectra. Because of the crucial role of the Coulomb forces, we speculate that fluids made of neutral quasiparticles such as magnons (if their hydrodynamic regime is realized [63, 64]) promise to be better candidates for convection in solid-state materials. It is tempting to suggest that phonon fluids [2, 65–68] might also demonstrate convective instability. It is not clear, however, whether the analogy with conventional fluids is complete and the equivalent of buoyancy forces is present.

P.O.S. acknowledges the support through the Yale Prize Postdoctoral Fellowship in Condensed Matter Theory. E.V.G. acknowledges a collaboration within the Ukrainian-Israeli Scientific Research Program of the Ministry of Education and Science of Ukraine (MESU) and the Ministry of Science and Technology of the state of Israel (MOST). The work of I.A.S. was supported by the U.S. National Science Foundation under Grant No. PHY-1713950.

* pavlo.sukhachov@yale.edu

[1] R. Gurzhi, Minimum of resistance in impurity-free conductors, JETP **17**, 521 (1963).
[2] R. N. Gurzhi, Hydrodynamic effects in solids at low temperature, Sov. Phys. Uspekhi **11**, 255 (1968).
[3] L. W. Molenkamp and M. J. M. de Jong, Observation of Knudsen and Gurzhi transport regimes in a two-dimensional wire, Solid State Electron. **37**, 551 (1994).
[4] M. J. De Jong and L. W. Molenkamp, Hydrodynamic electron flow in high-mobility wires,

Phys. Rev. B **51**, 13389 (1995).
[5] P. J. W. Moll, P. Kushwaha, N. Nandi, B. Schmidt, and A. P. Mackenzie, Evidence for hydrodynamic electron flow in $PdCoO_2$, Science **351**, 1061 (2016).
[6] J. Crossno, J. K. Shi, K. Wang, X. Liu, A. Harzheim, A. Lucas, S. Sachdev, P. Kim, T. Taniguchi, K. Watanabe, T. A. Ohki, and K. C. Fong, Observation of the Dirac fluid and the breakdown of the Wiedemann-Franz law in graphene, Science **351**, 1058 (2016).
[7] F. Ghahari, H.-Y. Xie, T. Taniguchi, K. Watanabe, M. S. Foster, and P. Kim, Enhanced Thermoelectric Power in Graphene: Violation of the Mott Relation by Inelastic Scattering, Phys. Rev. Lett. **116**, 136802 (2016).
[8] R. Krishna Kumar, D. A. Bandurin, F. M. D. Pellegrino, Y. Cao, A. Principi, H. Guo, G. H. Auton, M. Ben Shalom, L. A. Ponomarenko, G. Falkovich, K. Watanabe, T. Taniguchi, I. V. Grigorieva, L. S. Levitov, M. Polini, and A. K. Geim, Superballistic flow of viscous electron fluid through graphene constrictions, Nat. Phys. **13**, 1182 (2017).
[9] A. I. Berdyugin, S. G. Xu, F. M. D. Pellegrino, R. Krishna Kumar, A. Principi, I. Torre, M. Ben Shalom, T. Taniguchi, K. Watanabe, I. V. Grigorieva, M. Polini, A. K. Geim, and D. A. Bandurin, Measuring Hall viscosity of graphene's electron fluid, Science **364**, 162 (2019).
[10] D. A. Bandurin, A. V. Shytov, L. S. Levitov, R. K. Kumar, A. I. Berdyugin, M. Ben Shalom, I. V. Grigorieva, A. K. Geim, and G. Falkovich, Fluidity onset in graphene, Nat. Commun. **9**, 4533 (2018).
[11] M. J. H. Ku, T. X. Zhou, Q. Li, Y. J. Shin, J. K. Shi, C. Burch, L. E. Anderson, A. T. Pierce, Y. Xie, A. Hamo, U. Vool, H. Zhang, F. Casola, T. Taniguchi, K. Watanabe, M. M. Fogler, P. Kim, A. Yacoby, and R. L. Walsworth, Imaging viscous flow of the Dirac fluid in graphene, Nature **583**, 537 (2020).
[12] J. A. Sulpizio, L. Ella, A. Rozen, J. Birkbeck, D. J. Perello, D. Dutta, M. Ben-Shalom, T. Taniguchi, K. Watanabe, T. Holder, R. Queiroz, A. Principi, A. Stern, T. Scaffidi, A. K. Geim, and S. Ilani, Visualizing Poiseuille flow of hydrodynamic electrons, Nature **576**, 75 (2019).
[13] A. Lucas and K. C. Fong, Hydrodynamics of electrons in graphene, J. Phys. Condens. Matter **30**, 053001 (2018).
[14] B. N. Narozhny, Electronic hydrodynamics in graphene, Ann. Phys. (N.Y.). **411**, 167979 (2019).
[15] I. Torre, A. Tomadin, A. K. Geim, and M. Polini, Nonlocal transport and the hydrodynamic shear viscosity in graphene, Phys. Rev. B **92**, 165433 (2015).
[16] F. M. D. Pellegrino, I. Torre, A. K. Geim, and M. Polini, Electron hydrodynamics dilemma: Whirlpools or no whirlpools, Phys. Rev. B **94**, 155414 (2016).
[17] L. Levitov and G. Falkovich, Electron viscosity, current vortices and negative nonlocal resistance in graphene, Nat. Phys. **12**, 672 (2016).
[18] G. Falkovich and L. Levitov, Linking Spatial Distributions of Potential and Current in Viscous Electronics, Phys. Rev. Lett. **119**, 066601 (2017).
[19] S. Danz and B. N. Narozhny, Vorticity of viscous electronic flow in graphene, 2D Mater. **7**, 035001 (2020).
[20] H. Guo, E. Ilseven, G. Falkovich, and L. S. Levitov, Higher-than-ballistic conduction of viscous electron flows, Proc. Natl. Acad. Sci. U.S.A. **114**, 3068 (2017).
[21] A. Tomadin and M. Polini, Theory of the plasma-wave photoresponse of a gated graphene sheet, Phys. Rev. B **88**, 205426 (2013).
[22] D. Svintsov, V. Vyurkov, V. Ryzhii, and T. Otsuji, Hydrodynamic electron transport and nonlinear waves in graphene, Phys. Rev. B **88**, 245444 (2013).
[23] D. Svintsov, Emission of plasmons by drifting Dirac electrons: A hallmark of hydrodynamic transport, Phys. Rev. B **100**, 195428 (2019).
[24] C. B. Mendl, M. Polini, and A. Lucas, Coherent terahertz radiation from a nonlinear oscillator of viscous electrons, Appl. Phys. Lett. **118**, 013105 (2019).
[25] J. Gooth, F. Menges, N. Kumar, V. Süβ, C. Shekhar, Y. Sun, U. Drechsler, R. Zierold, C. Felser, and B. Gotsmann, Thermal and electrical signatures of a hydrodynamic electron fluid in tungsten diphosphide, Nat. Commun. **9**, 4093 (2018).
[26] M. I. Katsnelson, *Graphene: Carbon in Two Dimensions* (Cambridge University Press, Cambridge, U.K., 2012).
[27] N. P. Armitage, E. J. Mele, and A. Vishwanath, Weyl and Dirac semimetals in three-dimensional solids, Rev. Mod. Phys. **90**, 015001 (2018).
[28] E. V. Gorbar, V. A. Miransky, I. A. Shovkovy, and P. O. Sukhachov, *Electronic Properties of Dirac and Weyl Semimetals* (World Scientific, Singapore, 2021).
[29] Z. K. Liu, B. Zhou, Y. Zhang, Z. J. Wang, H. M. Weng, D. Prabhakaran, S.-K. Mo, Z. X. Shen, Z. Fang, X. Dai, Z. Hussain, and Y. L. Chen, Discovery of a three-dimensional topological dirac semimetal, Na_3Bi, Science **343**, 864 (2014).
[30] S.-Y. Xu, C. Liu, S. K. Kushwaha, R. Sankar, J. W. Krizan, I. Belopolski, M. Neupane, G. Bian, N. Alidoust, T.-R. Chang, H.-T. Jeng, C.-Y. Huang, W.-F. Tsai, H. Lin, P. P. Shibayev, F.-C. Chou, R. J. Cava, and M. Z. Hasan, Observation of Fermi arc surface states in a topological metal, Science **347**, 294 (2015).
[31] Z. K. Liu, J. Jiang, B. Zhou, Z. J. Wang, Y. Zhang, H. M. Weng, D. Prabhakaran, S.-K. Mo, H. Peng, P. Dudin, T. Kim, M. Hoesch, Z. Fang, X. Dai, Z. X. Shen, D. L. Feng, Z. Hussain, and Y. L. Chen, A stable three-dimensional topological Dirac semimetal Cd3As2, Nat. Mater. **13**, 677 (2014).
[32] M. Neupane, S.-Y. Xu, R. Sankar, N. Alidoust, G. Bian, C. Liu, I. Belopolski, T.-R. Chang, H.-T. Jeng, H. Lin, A. Bansil, F. Chou, and M. Z. Hasan, Observation of a three-dimensional topological Dirac semimetal phase in high-mobility Cd_3As_2, Nat. Commun. **5**, 3786 (2014).
[33] S. Borisenko, Q. Gibson, D. Evtushinsky, V. Zabolotnyy, B. Büchner, and R. J. Cava, Experimental Realization of a Three-Dimensional Dirac Semimetal, Phys. Rev. Lett. **113**, 027603 (2014).
[34] S.-Y. Xu, I. Belopolski, N. Alidoust, M. Neupane, G. Bian, C. Zhang, R. Sankar, G. Chang, Z. Yuan, C.-C. Lee, S.-M. Huang, H. Zheng, J. Ma, D. S. Sanchez, B. Wang, A. Bansil, F. Chou, P. P. Shibayev, H. Lin, S. Jia, and M. Z. Hasan, Discovery of a Weyl fermion semimetal and topological Fermi arcs, Science **349**, 613 (2015).
[35] S.-Y. Xu, I. Belopolski, D. S. Sanchez, C. Zhang, G. Chang, C. Guo, G. Bian, Z. Yuan, H. Lu, T.-R. Chang, P. P. Shibayev, M. L. Prokopovych, N. Alidoust, H. Zheng, C.-C. Lee, S.-M. Huang, R. Sankar, F. Chou, C.-H. Hsu, H.-T. Jeng, A. Bansil, T. Neupert, V. N. Strocov, H. Lin, S. Jia, and M. Z. Hasan, Experimental discovery of a topological Weyl semimetal state in TaP,

Sci. Adv. **1**, e1501092 (2015).
[36] B. Q. Lv, H. M. Weng, B. B. Fu, X. P. Wang, H. Miao, J. Ma, P. Richard, X. C. Huang, L. X. Zhao, G. F. Chen, Z. Fang, X. Dai, T. Qian, and H. Ding, Experimental Discovery of Weyl Semimetal TaAs, Phys. Rev. X **5**, 031013 (2015).
[37] B. Q. Lv, N. Xu, H. M. Weng, J. Z. Ma, P. Richard, X. C. Huang, L. X. Zhao, G. F. Chen, C. E. Matt, F. Bisti, V. N. Strocov, J. Mesot, Z. Fang, X. Dai, T. Qian, M. Shi, and H. Ding, Observation of Weyl nodes in TaAs, Nat. Phys. **11**, 724 (2015).
[38] L. X. Yang, Z. K. Liu, Y. Sun, H. Peng, H. F. Yang, T. Zhang, B. Zhou, Y. Zhang, Y. F. Guo, M. Rahn, D. Prabhakaran, Z. Hussain, S. K. Mo, C. Felser, B. Yan, and Y. L. Chen, Weyl semimetal phase in the non-centrosymmetric compound TaAs, Nat. Phys. **11**, 728 (2015).
[39] N. Xu, H. M. Weng, B. Q. Lv, C. E. Matt, J. Park, F. Bisti, V. N. Strocov, D. Gawryluk, E. Pomjakushina, K. Conder, N. C. Plumb, M. Radovic, G. Autès, O. V. Yazyev, Z. Fang, X. Dai, T. Qian, J. Mesot, H. Ding, and M. Shi, Observation of Weyl nodes and Fermi arcs in tantalum phosphide, Nat. Commun. **7**, 11006 (2016).
[40] S. Y. Xu, N. Alidoust, I. Belopolski, Z. Yuan, G. Bian, T. R. Chang, H. Zheng, V. N. Strocov, D. S. Sanchez, G. Chang, C. Zhang, D. Mou, Y. Wu, L. Huang, C. C. Lee, S. M. Huang, B. Wang, A. Bansil, H. T. Jeng, T. Neupert, A. Kaminski, H. Lin, S. Jia, and M. Z. Hasan, Discovery of a Weyl fermion state with Fermi arcs in niobium arsenide, Nat. Phys. **11**, 748 (2015).
[41] J.-R. Soh, F. de Juan, M. G. Vergniory, N. B. M. Schröter, M. C. Rahn, D. Y. Yan, J. Jiang, M. Bristow, P. A. Reiss, J. N. Blandy, Y. F. Guo, Y. G. Shi, T. K. Kim, A. McCollam, S. H. Simon, Y. Chen, A. I. Coldea, and A. T. Boothroyd, Ideal Weyl semimetal induced by magnetic exchange, Phys. Rev. B **100**, 201102(R) (2019).
[42] J.-Z. Ma, S. M. Nie, C. J. Yi, J. Jandke, T. Shang, M. Y. Yao, M. Naamneh, L. Q. Yan, Y. Sun, A. Chikina, V. N. Strocov, M. Medarde, M. Song, Y.-M. Xiong, G. Xu, W. Wulfhekel, J. Mesot, M. Reticcioli, C. Franchini, C. Mudry, M. Müller, Y. G. Shi, T. Qian, H. Ding, and M. Shi, Spin fluctuation induced Weyl semimetal state in the paramagnetic phase of $EuCd_2As_2$, Sci. Adv. **5**, eaaw4718 (2019).
[43] E. Liu, Y. Sun, N. Kumar, L. Meuchler, A. Sun, L. Jiao, S.-Y. Yang, D. Liu, A. Liang, Q. Xu, J. Kroder, V. Seuss, H. Borrmann, C. Shekhar, Z. Wang, C. Xi, W. Wang, W. Schnelle, S. Wirth, Y. Chen, S. T. B. Goennenwein, and C. Felser, Giant anomalous Hall effect in a ferromagnetic Kagome-lattice semimetal, Nat. Phys. **14**, 1125 (2017).
[44] Q. Xu, E. Liu, W. Shi, L. Muechler, J. Gayles, C. Felser, and Y. Sun, Topological surface Fermi arcs in the magnetic Weyl semimetal $Co_3Sn_2S_2$, Phys. Rev. B **97**, 235416 (2018).
[45] Q. Wang, Y. Xu, R. Lou, Z. Liu, M. Li, Y. Huang, D. Shen, H. Weng, S. Wang, and H. Lei, Large intrinsic anomalous Hall effect in half-metallic ferromagnet $Co_3Sn_2S_2$ with magnetic Weyl fermions, Nat. Commun. **9**, 3681 (2018).
[46] M. Mendoza, H. J. Herrmann, and S. Succi, Preturbulent Regimes in Graphene Flow, Phys. Rev. Lett. **106**, 156601 (2011).
[47] A. Gabbana, M. Polini, S. Succi, R. Tripiccione, and F. M. D. Pellegrino, Prospects for the detection of electronic pre-turbulence in graphene, Phys. Rev. Lett. **121**, 236602 (2018).
[48] D. Di Sante, J. Erdmenger, M. Greiter, I. Matthaiakakis, R. Meyer, D. R. Fernández, R. Thomale, E. van Loon, and T. Wehling, Turbulent hydrodynamics in strongly correlated Kagome metals, Nat. Commun. **11**, 3997 (2020).
[49] O. Furtmaier, M. Mendoza, I. Karlin, S. Succi, and H. J. Herrmann, Rayleigh-Bénard instability in graphene, Phys. Rev. B **91**, 085401 (2015).
[50] H. Benard, Les tourbillons cellulaires dans une nappe liquide, Rev. Gen. des Sci. Pures Appl. **11**, 1261 (1900).
[51] L. Rayleigh, On the convective currents in a horizontal layer of fluid when the higher temperature is on the under side, Philos. Mag. **32**, 529 (1916).
[52] Not only is the bulk viscosity negligible, but it would not play any significant role for the convective instability because the Coulomb forces strongly suppress compressions and expansions of the electron fluid.
[53] A. Principi, G. Vignale, M. Carrega, and M. Polini, Bulk and shear viscosities of the two-dimensional electron liquid in a doped graphene sheet, Phys. Rev. B **93**, 125410 (2016).
[54] P. S. Alekseev, Negative Magnetoresistance in Viscous Flow of Two-Dimensional Electrons, Phys. Rev. Lett. **117**, 166601 (2016).
[55] L. D. Landau and E. M. Lifshitz, *Fluid Mechanics* (Butterworth-Heinemann, Oxford, 2013).
[56] S. Chandrasekhar, *Hydrodynamic and Hydromagnetic Stability*, Dover Books on Physics Series (Dover, New York, 1981).
[57] See Supplemental Material for details of the derivations of the steady-state solutions and the convective threshold. Supplemental Material contains Refs. [69–73].
[58] N. Kumar, Y. Sun, N. Xu, K. Manna, M. Yao, V. Süss, I. Leermakers, O. Young, T. Förster, M. Schmidt, H. Borrmann, B. Yan, U. Zeitler, M. Shi, C. Felser, and C. Shekhar, Extremely high magnetoresistance and conductivity in the type-II Weyl semimetals WP_2 and MoP_2, Nat. Commun. **8**, 1642 (2017).
[59] One might naively suggest that convection could be still observed in thin films $L \ll \pi/q_{\rm TF}$. However, a small thickness of the slab makes external forces and thermal gradients less efficient [see Eqs. (19) and (24)].
[60] To accommodate even extreme possibilities, we extend the range of the Fermi energies down to the unrealistically small $\mu_0 = 1$ meV.
[61] M. S. Shur, *GaAs Devices and Circuits* (Springer, New York, 1987).
[62] M. Dyakonov and M. Shur, Shallow water analogy for a ballistic field effect transistor: New mechanism of plasma wave generation by dc current, Phys. Rev. Lett. **71**, 2465 (1993).
[63] E. Iacocca and M. A. Hoefer, Perspectives on spin hydrodynamics in ferromagnetic materials, Phys. Lett. A **383**, 125858 (2019).
[64] C. Ulloa, A. Tomadin, J. Shan, M. Polini, B. J. van Wees, and R. A. Duine, Nonlocal Spin Transport as a Probe of Viscous Magnon Fluids, Phys. Rev. Lett. **123**, 117203 (2019).
[65] K. Nil'sen and B. L. Shklovskii, Nonlinear thermal conductivity of dielectrics in the region of viscous flow of a phonon gas, Sov. Phys. Solid State **10**, 2857 (1969).

[66] A. Cepellotti, G. Fugallo, L. Paulatto, M. Lazzeri, F. Mauri, and N. Marzari, Phonon hydrodynamics in two-dimensional materials, Nat. Commun. **6**, 6400 (2015).
[67] S. Lee and X. Li, Hydrodynamic phonon transport: past, present and prospects, in *Nanoscale Energy Transp.* (IOP Publishing, Bristol, U.K., 2020) pp. 1–1 to 1–26.
[68] Y. Machida, N. Matsumoto, T. Isono, and K. Behnia, Phonon hydrodynamics and ultrahigh-room-temperature thermal conductivity in thin graphite, Science **367**, 309 (2019).
[69] P. Kovtun and A. Ritz, Universal conductivity and central charges, Phys. Rev. D **78**, 066009 (2008).
[70] S. A. Hartnoll, Theory of universal incoherent metallic transport, Nat. Phys. **11**, 54 (2015).
[71] K. Landsteiner, Y. Liu, and Y.-W. W. Sun, Negative magnetoresistivity in chiral fluids and holography, J. High Energy Phys. **2015** (3), 127.
[72] R. A. Davison, B. Goutéraux, and S. A. Hartnoll, Incoherent transport in clean quantum critical metals, J. High Energy Phys. **2015** (10), 112.
[73] S. A. Hartnoll, P. K. Kovtun, M. Müller, and S. Sachdev, Theory of the Nernst effect near quantum phase transitions in condensed matter and in dyonic black holes, Phys. Rev. B **76**, 144502 (2007).